

Low-frequency modes in vitreous silica

U. Buchenau and M. Prager

*Institut für Festkörperforschung, Kernforschungsanlage Jülich G.m.b.H., Postfach 1913, D-5170 Jülich,
Federal Republic of Germany*

N. Nücker

*Institut für Nukleare Festkörperphysik, Kernforschungszentrum Karlsruhe, Postfach 3640, D-7500 Karlsruhe,
Federal Republic of Germany*

A. J. Dianoux

Institut Laue-Langevin, F-38042 Grenoble Cédex, France

N. Ahmad and W. A. Phillips

Cavendish Laboratory, University of Cambridge, Madingley Road, Cambridge CB3 0HE, England, United Kingdom

(Received 9 June 1986)

Measurements of the elastic and inelastic neutron scattering from vitreous silica in the frequency range 0.3 to 4 THz and with scattering vectors in the range 0.2 to 5.3 Å⁻¹ are analyzed in conjunction with heat-capacity measurements on the same samples to provide a microscopic description of low-frequency vibrational modes. The results show that additional harmonic excitations coexist with sound waves below 1 THz, and that these excitations correspond to relative rotation of SiO₄ tetrahedra.

I. INTRODUCTION

The most marked differences between vibrational states in glasses and crystals occur at low frequencies, typically below 3 THz (100 cm⁻¹), and it is in this part of the frequency spectrum where the most dramatic changes occur in passing from the glass to the liquid state. Although these states have been extensively studied, there is no generally agreed microscopic description even in vitreous silica, the most heavily studied of all.

These vibrational states contribute to the heat capacity $C(T)$ in the temperature range 2 to 20 K, and experiments in SiO₂ indicate a density of states larger by a factor of 7 than calculated from measured sound velocities.¹ Infrared and Raman experiments can be used to probe these states but the most detailed information is provided by inelastic neutron scattering. In a previous publication,² preliminary results at frequencies in the range 0.3 < ν < 2.5 THz and with scattering vectors Q up to 3 Å⁻¹ indicated that in silica these states could be described as rotations of SiO₄ tetrahedra. In the present paper more extensive neutron experiments are described which extend the range of Q to 5.3 Å⁻¹, together with measurements of $C(T)$ in the range between 2 and 20 K on the same material. A more detailed analysis than that given in Ref. 2 allows a more complete description of the vibrational states, and also provides a way of choosing between the different models that have been proposed for the origin of these states.

The remainder of the paper is divided into three sections. Section II describes the experiments and data processing, while Sec. III gives a detailed analysis. This section is divided into five parts: calculation of the density

of states, comparison of the inelastic scattering for simple models, identification of the vibrational modes, comparison with the modes of crystalline silicas, and a critical examination of other models. Basic conclusions are given in Sec. IV.

II. MEASUREMENTS AND DATA ANALYSIS

The sample was a silica glass made out of natural quartz (Heralux from Heraeus at Hanau) with an OH content of ~130 ppm. For neutron scattering a tube of 16 mm diameter, 1-mm wall thickness, and about 100 mm long was used with a scattering probability for thermal neutrons of 12%.

The measurements were done on two time-of-flight spectrometers. The first was the IN6 at the High Flux Reactor of the Institut Laue-Langevin at Grenoble which is placed at a neutron guide of the cold source. The wavelength of the incoming neutrons was 5.1 Å. Measurements were carried out at three temperatures (50, 100, and 290 K) in the standard cryostat of the spectrometer. Empty cryostat measurements were done separately. The detector calibration was determined using a vanadium sample. In addition, the vanadium run was used to judge the "cleanness" of the low-frequency energy gain region.

To keep contamination from the tail of the elastic line small compared to the inelastic sample signal, it was necessary to restrict the measurement to frequencies above 150 GHz (more than six times the full resolution width away from the elastic line).

The measurement was extended to higher momentum-

transfer values by a room-temperature measurement with neutrons of 2.5 Å wavelength at the time-of-flight spectrometer SV22 at Jülich. This instrument is situated at a thermal beam tube of the DIDO reactor. It has a double monochromator and consequently a very clean background even very near to the elastic line. On the SV22 measurements from 400 GHz upwards were possible.

Elastic scattering data obtained on the two spectrometers was supplemented by measurements on the triple axis spectrometer SV4 at Jülich. All three sets of results were in good agreement with each other and with published data³ after inclusion of the measured Debye-Waller factor e^{-2W} , obtained from a comparison of the elastic intensity at three temperatures. Using the high-temperature approximation to W gave an effective Debye temperature of 370 K, smaller than the value of 494 K obtained from the sound velocities. At room temperature the Debye-Waller factor was 0.94 at 2 \AA^{-1} .

The Debye-Waller factor can be used to extrapolate to larger values of Q the influence of multiphonon scattering, which increases approximately⁴ as Q^4 . The estimate showed that multiphonon scattering is still negligibly small as compared to the one phonon scattering at room temperature below 4 THz.

Multiple scattering is evident at small Q . The experience of low-frequency scattering from polycrystals⁵ shows that multiple scattering is essentially Q independent, which allows the zero Q contribution to be subtracted from both elastic and inelastic data.

The intensity of the elastic line was used to calibrate inelastic measurements: Normalized inelastic intensities measured on different spectrometers were identical within experimental error in the regions of overlap. Absolute inelastic intensities were also obtained by reference to the elastic structure factor $S_0(Q)$ [$S_0(Q) = S(Q, 0) = S(Q)e^{-2W}$] in two different ways.

(i) The first peak in $S_0(Q)$ was calibrated by reference to published³ data on SiO_2 which allows the absolute height to be related to the high- Q limit. An effective number of scattering atoms was deduced from this incoherent limit.

(ii) For the model of five tetrahedra, described in Sec. III B, which contains sufficient atoms to describe the main features of $S_0(Q)$, the calculated $S_0(Q)$ was compared directly to the experimental elastic scattering.

Both methods were in essential agreement (difference 6%) although the first is to be preferred as being less model sensitive. The Debye-Waller factor was taken into account during normalization, but in practice this correction was unimportant at the small values of Q involved in a scaling of the first peak of $S_0(Q)$.

The heat capacity of a small (134 mg) sample cut from the tube was measured, using a standard pulse technique,⁶ over the temperature range 1.5 to 20 K. A flat surface was ground on the silica which was then attached to a silicon-on-sapphire bolometer⁷ using silicon oil. The additional heat capacity of the bolometer and supporting wires decreased from 25% of the total at 1.5 K to 10% at 20 K. Values of C , believed accurate to 3%, are in close agreement with measurements on Amersil,⁸ but are about 20% lower than results on Spectrosil-B.⁹

III. DISCUSSION

A. Density of states

As shown in Ref. 2, the excitations above 0.5 THz are essentially harmonic vibrations. This can be seen from the temperature dependence of the inelastic signal. In principle, the scattering from a two-level state is temperature independent when the temperature exceeds the corresponding level splitting, while the scattering from harmonic vibrations is proportional to the Bose factor n_b (for our frequencies and temperatures essentially proportional to temperature). Except for frequencies below 0.5 THz at 290 K all data scale with n_b . The nonharmonic contribution, reminiscent of that observed¹⁰ in Raman scattering in SiO_2 , will be the subject of a separate publication.

In the range above 0.5 THz both neutron and heat-capacity data indicate a density of vibrational states $g(\nu)$ which is considerably higher than the Debye value. Normalizing the densities of states to unity, so that

$$\int g(\nu) d\nu = 1,$$

the Debye value is given by

$$g_D(\nu) = \frac{4\pi V}{3} \left[\frac{1}{v_l^3} + \frac{2}{v_t^3} \right] \nu^2, \quad (1)$$

where v_l and v_t are the longitudinal and transverse sound velocities, and V is the average atomic volume.

The one-phonon scattering cross section is given by¹¹

$$\frac{d^2\sigma^{(1)}}{d\Omega d\nu} = \frac{k_f}{k_i} \frac{3\hbar N}{4\pi} \frac{g(\nu)}{\nu} n_B I^{(1)}(Q), \quad (2)$$

where $\mathbf{Q} = \mathbf{k}_f - \mathbf{k}_i$, where \mathbf{k}_f and \mathbf{k}_i are the final and incident neutron wave vectors, n_B the Bose factor, N the number of atoms, and

$$I^{(1)}(Q) = \left| \sum_j b_j e^{-W_j} e^{i\mathbf{Q} \cdot \mathbf{R}_j} (\mathbf{Q} \cdot \mathbf{e}_j) / M_j^{1/2} \right|^2, \quad (3)$$

where b_j is the coherent scattering length, \mathbf{R}_j the position vector, M_j the mass, and \mathbf{e}_j the displacement amplitude of atom j . The polarization vectors are related to the actual displacements \mathbf{u}_j by $\mathbf{u}_j = M_j^{1/2} \mathbf{e}_j$, and normalized so that $\sum_j \mathbf{e}_j^2 = 1$.

On the assumption that the Q dependence of $I^{(1)}(Q)$ is the same for all modes in this frequency range, $g(\nu)$ can be obtained by scaling the inelastic intensities to give a common curve, shown in Fig. 3. The close agreement between scaled results at different frequencies supports the initial assumption in the range $0.3 < \nu < 2$ THz. Derived values of the density of states, given directly by the scaling factor, are shown in Fig. 1. The proportionality factor depends on the model used to fit the Q dependence of $I^{(1)}(Q)$ but as discussed in Sec. III B, all models oscillate around an underlying Q^2 dependence. The Q range of the present work was large enough to suppress the influence of the Q oscillations on the determination of $g(\nu)$ within a few percent. The only model assumption left in the neutron $g(\nu)$ curve in Fig. 1 is that of a pure oxygen motion. [A model with pure Si motion yields $g(\nu)$ larger by fac-

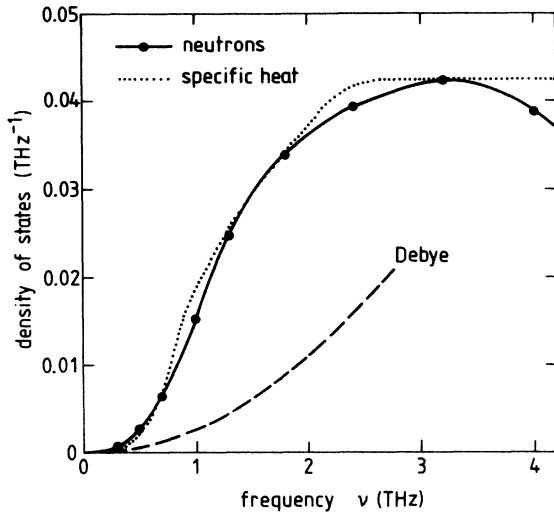


FIG. 1. Density of states $g(\nu)$ in vitreous silica derived (a) from the scaling factor used to bring the inelastic neutron intensities to the common curve shown in Fig. 3 and (b) from the heat capacity.

tors 3.3 and equal amplitudes of both atoms increases $g(\nu)$ by a factor of 1.5. This results from differences in scattering lengths and masses entering Eq. (3).]

Figure 2 compares the heat capacity calculated from the density of vibrational states in Fig. 1 to the measured data. The agreement to within 10% is smaller than the estimated error in the normalization factor (connected with the accurate determination of multiple scattering and the Debye-Waller factor) of about 20%. The assumption of predominant oxygen motion is confirmed. The general form of the two curves is in good agreement. When plotted in Fig. 2 as C/T^3 against T , the results show a peak at 11 K which in turn indicates a density of states $g(\nu)$ which first increases more rapidly than ν^2 and then less

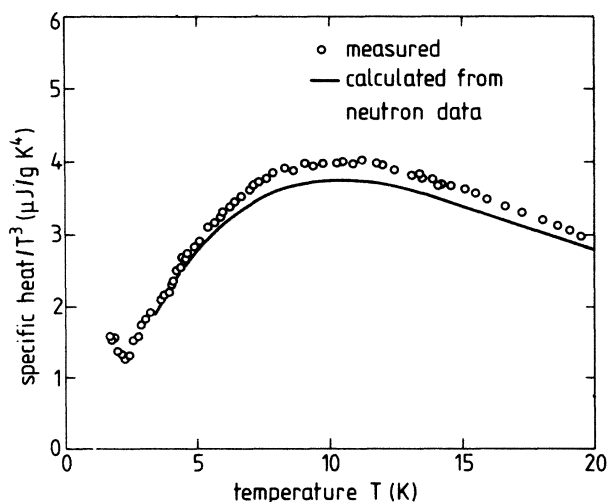


FIG. 2. Specific heat C of vitreous silica plotted as C/T^3 against temperature T . The points are experimental data and the line is calculated from the neutron data shown in Fig. 1.

rapidly as shown in Fig. 1. The neutron data do not determine $g(\nu)$ below 0.3 THz, where nonharmonic excitations are important, but $g(\nu)/\nu^2$ was smoothly extrapolated to the Debye limit for calculation of $C(T)$.

It is interesting to compare the form of $g(\nu)$ shown in Fig. 1 with that deduced from neutron data using the incoherent approximation. Although this approximation fails at very low frequencies, where the vibrational amplitudes show a large degree of coherent motion, both Leadbetter *et al.*¹² ($Q < 10 \text{ \AA}^{-1}$) and Carpenter and Price¹³ ($Q < 16 \text{ \AA}^{-1}$) have presented data at frequencies down to 3 THz (100 cm^{-1} or 12.4 meV). The data can be directly compared if the earlier data of Leadbetter *et al.* is corrected for multiphonon scattering and the curve normalized to unity. Surprisingly, the earlier data of Leadbetter¹² agrees well with the absolute values derived from the heat capacity. Carpenter and Price, however, show that $g(\nu) < g_D(\nu)$ below 3 THz, in conflict with Fig. 1. However, the effect of the incoherent approximation must be examined more carefully before firm conclusions can be drawn.

B. Structural analysis

The variation with Q of the inelastic scattering as shown in Fig. 3 provides detailed information on vibrational modes. The data is most easily understood by first calculating the inelastic structure factor for a number of models of increasing complexity. For comparison, the elastic scattering is also calculated for the more complex models within the spirit of the quasicrystalline approach.¹⁴

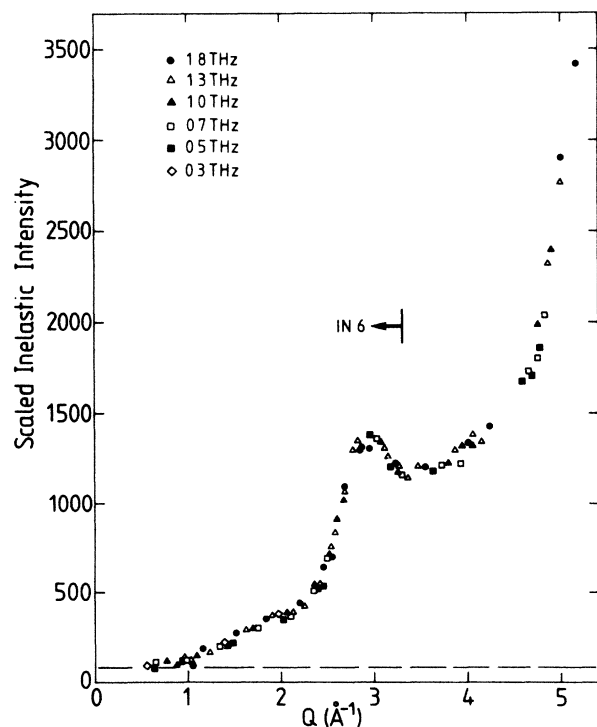


FIG. 3. Inelastic scattering intensities scaled to a common curve.

1. Sound waves

The effect of well-defined phase relationships between the motion of neighboring atoms can be examined by calculating the inelastic cross section for sound waves. In the limit $q \ll Q$, where q is the wave vector of the sound wave, Eqs. (2) and (3) give¹⁵

$$\frac{d^2\sigma^{(1)}}{d\Omega d\nu} = \frac{1}{2\pi} \frac{k_f}{k_i} \frac{hQ^2}{2M_{av}} n_b \frac{g_D(\nu)}{\nu} I^{(0)}(Q), \quad (4)$$

where M_{av} is the average atomic mass and

$$I^{(0)}(Q) = \left| \sum_j b_j e^{-W_j} e^{i\mathbf{Q}\cdot\mathbf{R}_j} \right|^2 \quad (5)$$

is proportional to the elastic structure factor. $I^{(1)}(Q)$ is therefore proportional to $Q^2 S_0(Q)$ and in SiO_2 would show a strong peak at 1.6 \AA^{-1} .

2. Single atom

The Einstein mode represents the opposite limit, where no coherent motion exists. In this case the only terms in Eq. (2) which contribute are the "self" terms, so that $I^{(1)}(Q)$ is proportional to Q^2 . In general, therefore, information on the nature of the vibrational modes is contained in the form of $I^{(1)}(Q)/Q^2$ and not in the general increase of $I^{(1)}(Q)$ as Q^2 .

3. Single tetrahedron

Both elastic and inelastic scattering can be calculated explicitly for molecules and small clusters.^{16,17} Ignoring Debye-Waller factors, the results obtained after averaging over angles are

$$I^{(0)}(Q) = \sum_{i,j} b_i b_j j_0(QR_{ij}) \quad (6)$$

and

$$I^{(1)}(Q) = \sum_{i,j} \left\{ \frac{1}{3} (\mathbf{e}_i \cdot \mathbf{e}_j) [j_0(QR_{ij}) + j_2(QR_{ij})] - (1/R_{ij})^2 (\mathbf{R}_{ij} \cdot \mathbf{e}_i) (\mathbf{R}_{ij} \cdot \mathbf{e}_j) j_2(QR_{ij}) \right\}, \quad (7)$$

where $R_{ij} = |\mathbf{R}_i - \mathbf{R}_j|$, j_0 and j_2 are Bessel functions, and both indices i and j run over all atoms.

The structure-independent part of $I^{(0)}(Q)$ at $Q=0$ is subtracted using a Gaussian function with a weight given by the average scattering of the atoms in a cavity containing the tetrahedron and the result normalized to give $S_0(Q)$. Maxima in $S_0(Q)$ at $Q=2.9$ and 5.2 \AA^{-1} are determined by the O-O distance of 2.6 \AA although the Si-O distance of 1.6 \AA gives an additional contribution which is responsible for the greater amplitude of the higher Q peak. Because the number of nearest neighbor O-O and Si-O separations in a single tetrahedron is the same as that for vitreous silica as a whole, changes in relative magnitudes of the two tetrahedron peaks in $S_0(Q)$ should be small when the calculation is extended to other structures. The calculated result for $S_0(Q)$ is shown in Fig. 6.

Although direct calculation using Eq. (7) [or Eq. (3) averaged numerically over angle] is needed to give the precise form of $I^{(1)}(Q)$, the main features of the results can be understood on the basis of an approximate form of Eq. (7). The sum $j_0(x) + j_2(x)$ can be written as $3j_1(x)/x$, so that the relative magnitudes of the two terms on the right-hand side of the Eq. (7) are given approximately by the ratio $j_1(x)/xj_2(x)$ for most combinations of the \mathbf{e}_j . For x larger than 2.5 the second term is more important, so that the peaks in $I^{(1)}(Q)$ are given by maxima in

$$-\sum_{i,j} (1/R_{ij})^2 (\mathbf{R}_{ij} \cdot \mathbf{e}_i) (\mathbf{R}_{ij} \cdot \mathbf{e}_j) j_2(QR_{ij}). \quad (8)$$

If $(\mathbf{R}_{ij} \cdot \mathbf{e}_i)$ and $(\mathbf{R}_{ij} \cdot \mathbf{e}_j)$ have the same sign ($\mathbf{e}_i \cdot \mathbf{e}_j > 0$) then, for a single R_{ij} , maxima in $I^{(1)}(Q)$ correspond to minima in $j_2(QR_{ij})$, and vice versa. It is straightforward to show that for pure rotation all terms in the summation of Eq. (8) are positive. For rotation of the tetrahedron about an axis passing through the Si atom only the O-O distance is relevant, giving peaks in $I^{(1)}(Q)/Q^2$ at approximately 2.7 and 5.3 \AA^{-1} . This is shown in the results of the complete calculation [using Eq. (3) and not Eq. (8)] in Fig. 5. It should also be noted that the relative heights of the two peaks in $I^{(1)}(Q)/Q^2$ is reversed from that seen in $S_0(Q)$.

Other kinds of motion give different forms of $I^{(1)}(Q)$. In general, distortion of the tetrahedron gives maxima where rotation gives small values. For example, the tetrahedral breathing mode gives maxima in $I^{(1)}(Q)/Q^2$ at maxima in j_2 because $\mathbf{e}_i \cdot \mathbf{e}_j < 0$ for all pairs of atoms. The wag mode gives smaller maxima at Q equal to 1.6 and 4.1 \AA^{-1} . A displacement of the complete tetrahedron will, by analogy with the sound wave calculation, give $I^{(1)}(Q)$ proportional to $Q^2 S_0(Q)$.

4. Paired tetrahedra

This nine-atom unit, illustrated in Fig. 4(b), is a first step towards accounting for neighboring atoms round the single tetrahedron of Sec. III B 3 and is the basic repeat unit of crystalline silicas. The calculated $S_0(Q)$ is shown in Fig. 6. The most significant result is the appearance of a peak at 1.6 \AA^{-1} , a feature of the bulk glass which has been the subject of much recent discussion.¹⁸ It can be identified as arising from the next-nearest-neighbor O-O distances of 4.5 \AA , although the Si-O and O-O nearest-neighbor contributions are important in determining the exact position of the peak. Changing the Si—O—Si bond angle from 180 to 154° (the mean value in the glass) broadens and moves the peak to slightly higher values of Q as expected. Contributions from Si-Si and Si-O distances above 1.6 \AA do not contribute significantly to $S_0(Q)$. The magnitude of the peak at 1.6 \AA^{-1} in Fig. 6 is of course low in comparison with the glass because the number of next-nearest neighbors is not representative of the bulk. Analysis of the five-tetrahedra model (Sec. III B 5 and Ref. 2) shows how this peak increases with the number of tetrahedra.

The inelastic scattering factor $I^{(1)}(Q)$ (Fig. 5), calculat-

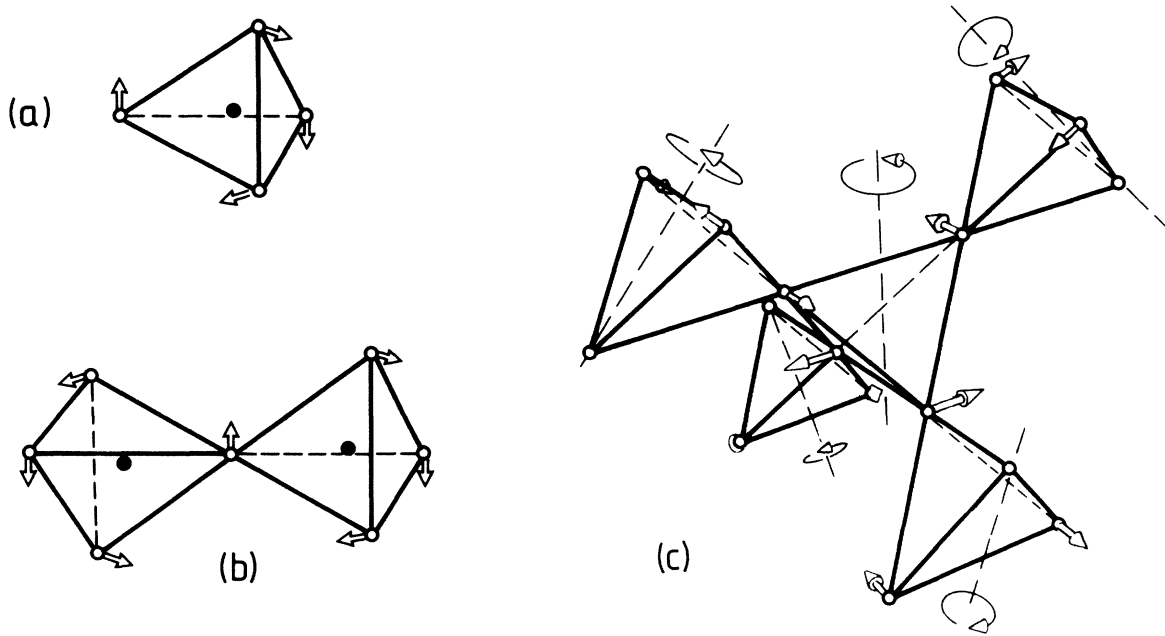


FIG. 4. Structural models used in the calculation (a) single tetrahedron, (b) pair of tetrahedra, and (c) five tetrahedra.

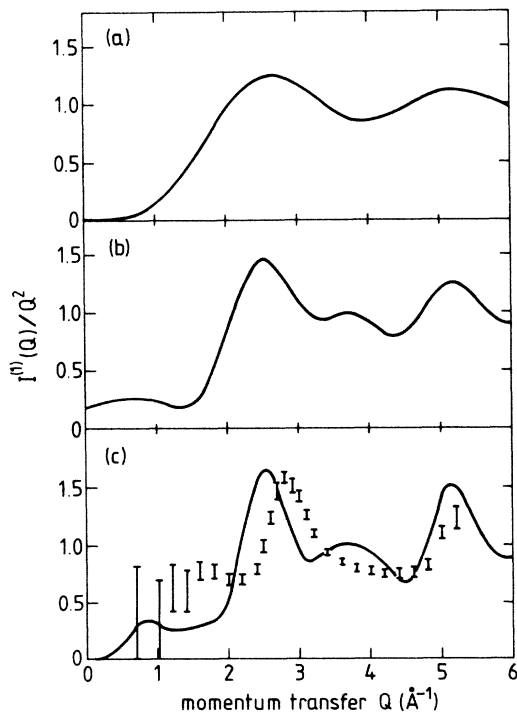


FIG. 5. Inelastic factor $I^{(1)}(Q)/Q^2$ normalized to 1 for $Q \rightarrow \infty$ for (a) rotation of a single tetrahedron, (b) selective rotation of two tetrahedra, and (c) the relative rotation of five. Also shown are experimental points with error bars derived from Fig. 3.

ed for a coupled rotation of both tetrahedra around two parallel axes through the Si atoms of the form shown in Fig. 4, shows similar features to that of a single tetrahedron. The peak in $I^{(0)}(Q)$ at 1.6 \AA^{-1} is not seen clearly in $I^{(1)}(Q)/Q^2$ because some of the relevant factors $(\mathbf{R}_{ij} \cdot \mathbf{e}_i)(\mathbf{R}_{ij} \cdot \mathbf{e}_j)$ are negative, with consequent cancellation between terms of opposite sign in Eq. (8).

The apparent shoulder at 3.8 \AA^{-1} in $I^{(1)}(Q)/Q^2$, not seen for a single tetrahedron, arises from the cancellation of contributions from different oxygen-oxygen second neighbors, an accidental coincidence that is easily destroyed by changes in the Si—O—Si bond angle or by different types of motion. For example, this peak almost vanishes if the central oxygen atom in the pair of tetrahedron has twice the amplitude of the others. The first peak in $S_0(Q)$ will be seen in $I^{(1)}(Q)/Q^2$ if the nine atoms have equivalent displacement (as in a sound wave) and for rigid rotation of both tetrahedra about any of the six noncentral oxygen atoms.

For purposes of comparison with experiment the most significant features of $I^{(1)}(Q)/Q^2$ are the exact positions of the two peaks at approximately 2.6 and 5.1 \AA^{-1} , their relative heights, and the width of both peaks. Taking the pair shown in Fig. 4(b) as a reference, none of these features is significantly changed by rotation about the Si—O—Si axis. By contrast, the position of the lower- Q peak is shifted to higher Q , and the higher- Q peak is considerably broadened when the Si—O—Si bond angle is increased to 154° , the average value in the glass. Increasing the amplitude of the central oxygen atom by a factor of 2 relative to the other 6, equivalent to rotation with slight

distortion of the tetrahedron, has little effect on the two peaks but reduces structure in the valley between them.

5. Five tetrahedra

This model has been discussed in some detail in an earlier publication.² Calculations based on a Si—O distance of 1.6 Å and an Si—O—Si bond angle of 180° are shown in Figs. 5 and 6. Features ascribed to oxygen-oxygen next-nearest neighbors are now stronger than for two tetrahedra. The width of the 2.6 Å⁻¹ peak in $I^{(1)}(Q)/Q^2$ becomes considerably smaller and begins to compare favorably with the experimental data. Similar trends, as a function of the Si—O—Si bond angle and relative displacements, are expected for this group of atoms as for a pair of tetrahedra.

C. Vibrational mode analysis of experimental results

In Ref. 2 the sound wave contribution to the inelastic scattering was subtracted before scaling the remaining contribution to obtain an excess density of states, a procedure which removes any sign of a peak at 1.6 Å⁻¹. However, comparison with Figs. 3 and 5(c) shows that this peak is not significant even without subtraction of a sound wave contribution. The neutron data cannot therefore demonstrate the presence or absence of sound

waves in this frequency range in the presence of the much larger density of non-Debye modes (Fig. 1). At higher frequencies where the condition $q \ll Q$ is not satisfied (assuming q can be defined) the characteristic sound wave signature $S_0(Q)$ in the inelastic intensity will be broadened unrecognizably. Evidence on the range of frequencies over which well-defined nondispersive sound waves exist must be sought in other experiments.

Nondispersive sound waves are known to exist at low frequencies from Brillouin scattering¹⁹ ($\nu < 30$ GHz) and phonon interference²⁰ ($\nu < 500$ GHz) experiments. Analysis of the thermal conductivity κ of SiO₂ based on this premise²¹ suggests that sound waves are reasonably well defined below 1 THz, but in order to explain the "plateau" in κ between 4 and 20 K the free path for transverse waves must be smaller than the wavelength at higher frequencies. Furthermore, the total density of states derived either from $C(T)$ or the neutron data suggests a value less than the Debye value above 4 THz, in direct contradiction to the postulate of nondispersive sound waves. This accumulated evidence indicates that well-defined nondispersive sound waves exist below 1 THz, but not at higher frequencies. Our analysis is consistent with this picture. (Longitudinal modes may exist above 1 THz but, contributing only 10% of the Debye density of states, can be ignored in the following analysis.)

The most noticeable features of all the data (Fig. 3) are the sharp rise to maxima at 2.9 and 5.1 Å⁻¹, both corresponding to peaks seen in $I^{(1)}(Q)$ of individual tetrahedra. Together with the absence of a strong peak at 1.6 Å⁻¹, this strongly suggests that the dominant motion in the frequency range 0.3 to 2 THz corresponds to coupled rotation of tetrahedra. Detailed fitting confirms this suggestion and the model calculation of $I^{(1)}(Q)$ allows an absolute value to be assigned to the neutron density of states (as described in Sec. IV A). This picture applies even below 0.5 THz where the larger concentration of coupled rotational modes mask the sound wave contribution. The focus of this analysis is on the O—O nearest-neighbor distance giving peaks in the measured $S_0(Q)$ and $I^{(1)}(Q)/Q^2$ at 2.9 and 5.1 Å⁻¹. Although the peak found at 1.5 Å⁻¹ for the pair and five tetrahedra models is difficult to reproduce in large-scale random cluster²² models, the other two peaks are preserved and in general become better defined as the number of tetrahedra increases. This sharpening is significant from our point of view because we can duplicate the sharp rise at 5 Å⁻¹ in the inelastic intensity [or equivalently the sharp peak in $I^{(1)}(Q)/Q^2$] in model calculations only by maintaining the Si—O—Si bond angle close to 180°. Better agreement with experiment is also obtained if the Si—O bond length is decreased from 1.60 to 1.54 Å, a change which is associated with increases in the Si—O—Si bond angle.^{21,23} We expect that calculations carried out for coupled rotation of tetrahedra in larger models would give a sharp rise in $I^{(1)}(Q)$ without this constraint on the bond angle. At frequencies above 2.5 THz the increase of $I^{(1)}(Q)$ becomes less sharp, and the peak at 2.8 Å⁻¹ less well defined, a trend consistent either with the idea that with increasing frequency tetrahedra in which the Si—O—Si bond angle is less than 180° become increasingly involved in the

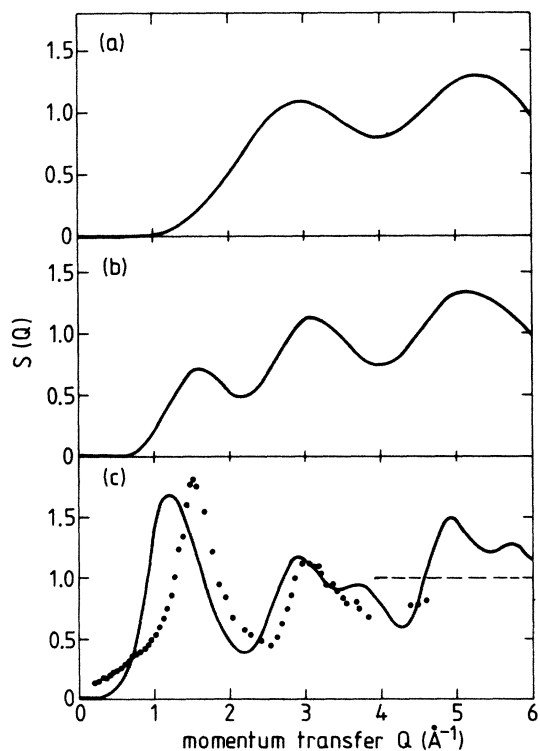


FIG. 6. $S(Q)$ for (a) single tetrahedron, (b) pair of tetrahedra, and (c) five tetrahedra. Also shown are scaled experimental points.

motion or with motion restricted to a smaller number of atoms.

It is important to be precise about the kind of information on localization provided by $I^{(1)}(Q)$. For a bulk glass the summations in Eqs. (3), (6), and (7) are over all atoms in the solid (and therefore give selection rules in the crystal) and the result is averaged over time.^{22,24} In the disordered solid the average in Eqs. (6) and (7) contains contributions only for pairs of atoms which have correlated motion, and so, except at the lowest frequencies, only for close neighbors. A clear distinction must be made between the fact that $I^{(1)}(Q)$ can be interpreted in a local picture and the concept of phonon localization, which can be studied only indirectly through widths of peaks in $I^{(1)}(Q)/Q^2$.

D. Relation to crystalline silica

The structures of vitreous silica and the most common forms of crystalline silica are based on corner-sharing SiO_4 tetrahedra, and this similarity suggests that examination of local motion in the crystals will provide a useful comparison for the results of Sec. III C. A highly significant feature observed in crystals is the extremely wide range of zone boundary and zone-center modes.²⁵ In perfect crystals of quartz, for example, such frequencies range from 1.5 to 36 THz. At the microscopic levels, the modes above 15 THz can be classified in broad terms as stretching vibrations of the Si—O bonds, while those between 12 and 15 THz are dominated by distortion of the SiO_4 tetrahedra with the Si—O bond essentially constant in length. Below 12 THz the modes are either sound waves or involve the rotation of relatively undistorted tetrahedra.

Confirmation of this general picture comes from calculations of normal mode frequencies and displacements. In the frequency range relevant to this paper the most detailed analysis has been made of the modes at 4 and 6 THz in the low-temperature form of quartz, which soften near the α - β phase transformation temperature of 846 K. These modes clearly involve coupled rotation of SiO_4 tetrahedra.²⁶

Calculations of the phonon density of states in α quartz²⁷ and cristobalite²⁸ show that the densely spaced tetrahedral rotation and distortion modes give an almost constant density of states, which in quartz would occur for frequencies in the range 1.5 to 12 THz. Although a calculation in cristobalite²⁸ based on a two-parameter Born model gave incorrect values for zone-boundary frequencies, a more recent calculation²⁹ based on a modified Keating model which includes the three qualitatively important force constants (Si-O stretch, O-Si-O, and Si-O-Si bend), confirms the existence of low-frequency transverse acoustic zone-boundary modes. The important conclusion of this analysis of the vibrational modes is that the general form of the crystalline density of states, after broadening, would resemble that shown in Fig. 1, and also that vibrational modes corresponding to rotation of almost rigid tetrahedra can occur at frequencies below 2 THz in crystalline silica.

E. Comparison of models

A currently fashionable explanation for the form of the density of states needed to explain the peak in C/T^3 is based on fractals or fractional dimensionality.³⁰ Originally developed for polymeric materials, it has been extended to other glasses on the basis that all amorphous materials show a characteristic length scale L above which the solid is essentially homogeneous. This could, for example, be identified with the distance at which structure in the radial distribution function becomes small, or more precisely in polymers with the distance between crosslinks. For wavelengths greater than L , the system is three dimensional with the usual quadratic density of states, but at shorter wavelengths the dimensionality is reduced to a value close to unity, with a corresponding density of states that is only weakly frequency dependent. The crossover between the two regimes occurs at a frequency given by $\nu = v_s/L$, and it has been claimed that at this point the density of states increases above the Debye value, as it must to explain the peak in $C(T)/T^3$.

This idea is superficially attractive in that all amorphous solids show a peak in C/T^3 at a temperature which corresponds to vibrational frequencies given very approximately by v_s/L if L is taken in the range 0.5 to 1.0 nm. For example, the density of states in epoxy resins increases significantly above the Debye value at frequencies in the range 0.3–0.6 THz, which correspond to L approximately equal to 2 nm.

The results presented in this paper cast serious doubt on the fractal picture for three main reasons.

(i) The derived form of the low-frequency density of states in vitreous SiO_2 is similar to that of epoxy resins³¹ even though the structures are very different. Moreover, both calculation and experiment show a very similar form for $g(\nu)$ in cristobalite, where no one would suggest the fractal model should apply.

(ii) At higher frequencies the density of states in vitreous silica rises above the plateau to a peak at 12 THz.^{12,13} In epoxies the density of states shows not a plateau but a single broad peak.³¹ In neither material is there a frequency regime in which the density of states has a well-defined power-law dependence less than two. Attempts to fit C in this way capitalize on the insensitivity of $C(T)$ at low temperature to $g(\nu)$ at higher frequencies.

(iii) The inelastic neutron data show very clearly the existence of harmonic modes below 0.7 THz, where sound waves are known to exist, in addition to the nonharmonic two-level states important below 1 K. The fractal model makes a clear distinction between the three-dimensional properties and fractal behavior. If the increase of $g(\nu)$ at 0.3 THz in vitreous silica were to be attributed to the onset of fractal behavior the model would give a length scale of $L = v_s/\nu \sim 10$ nm. This is unreasonably large in comparison with the equivalent length of 2 nm in epoxies, which are much closer to one-dimensional solids.

In addition to the "fracton" model, the peak in C/T^3 has been explained in cristobalite, and by analogy in vitreous silica, as arising from transverse acoustic waves traveling on internal surfaces in the solid.³² These surfaces are claimed to be microtwin interfaces in the crystal, and

clusters in the glass. Twinning occurs as a result of the α - β transformation, which in turn is related to the soft mode identified as rotation of tetrahedra. In the absence of a detailed microscopic picture for the atomic displacements associated with the surface acoustic waves the results presented here can neither confirm nor repudiate this model which has, however, been criticized in other respects.³³

Neither of these two models satisfactorily explain the inelastic neutron experiments, which support a picture in which the large density of states between 0.5 and 3 THz result from modes in which almost rigid tetrahedra rotate relative to each other, as expected from a study of vibrational modes in crystalline silicas.

IV. CONCLUSIONS

The most important results of the analysis of the inelastic neutron intensity can be summarized as follows

(i) At any given frequency below 1 THz sound waves with a well-defined wave vector and constant velocity coexist with a second class of harmonic excitations.

(ii) A quantitative comparison of neutron and heat-capacity data shows that these additional excitations predominantly involve oxygen motion.

(iii) The form of $I^{(1)}(Q)$ indicates that these additional excitations can be represented as relative rotation of almost rigid tetrahedra.

These results, together with an analysis of vibrations in

crystalline quartz, lead us to propose the following picture for low-lying modes in vitreous silica. Nondispersive sound waves exist up to frequencies of approximately 1 THz ($q=2\times 10^9\text{ m}^{-1}$) although disorder in the solid gives a rapid decrease of the phonon mean-free path as this frequency is approached. In addition, disorder mixes modes which in the crystal would be described as the high- q part of the dispersive (transverse) acoustic branch to give a spread of frequencies about a mean of approximately 1 THz. Dispersion is important in giving a wide range of different modes in a narrow frequency range. Each normal mode, of course, contains a wide range of possible values of q , and so cannot be represented in a simple way.

This picture is firmly based on the inelastic neutron results above 0.3 THz, but it is interesting to speculate on what happens in the limit of zero frequency. The way in which frequencies can approach zero in a structure based on linked tetrahedra, and how the structure becomes locally unstable has been demonstrated both by considering the effect of the surrounding solid on a pair of tetrahedra³⁴ and by model calculations.³⁵ The resulting two-well potentials are consistent with what is known about tunneling states at low temperatures, and also with the microscopic motion described for low-frequency excitations in connection with the data. These results therefore give, for the first time, structural indications as to the nature of double-well potentials in glasses.

¹R. O. Pohl, in *Amorphous Solids—Low Temperature Properties*, Vol. 24 of *Topics in Current Physics*, edited by W. A. Phillips (Springer-Verlag, Berlin, 1981), p. 27.

²U. Buchenau, N. Nücker, and A. J. Dianoux, *Phys. Rev. Lett.* **53**, 2316 (1984).

³P. A. V. Johnson, A. C. Wright, and R. N. Sinclair, *J. Non-Cryst. Solids* **58**, 109 (1983); Y. Tanaka, N. Ohtoma, and M. Katahama, *J. Phys. Soc. Jpn.* **54**, 967 (1985).

⁴W. Marshall and S. W. Lovesey, *Theory of Thermal Neutron Scattering* (Oxford, Clarendon, 1971), p. 94.

⁵U. Buchenau, *Solid State Commun.* **32**, 1329 (1979).

⁶R. Bachmann, F. J. DiSalvo, T. H. Geballe, R. L. Green, R. E. Howard, C. N. King, H. C. Kirsch, K. N. Lee, R. E. Schwal, H. U. Thomas, and R. B. Zubeck, *Rev. Sci. Instrum.* **43**, 205 (1972).

⁷S. R. Early, F. Hellman, J. Marshall, and T. H. Geballe, *Physica* **107B&C**, 327 (1981).

⁸P. Flubacher, A. J. Leadbetter, J. A. Morrison, and B. P. Stoicheff, *J. Phys. Chem. Solids* **12**, 53 (1959).

⁹O. B. Wright and W. A. Phillips, *Philos. Mag.* **B 50**, 63 (1984).

¹⁰G. Winterling, *Phys. Rev. B* **12**, 2432 (1975).

¹¹U. Buchenau, *Z. Phys. B* **58**, 181 (1985) [Eq. (19)].

¹²F. L. Galeener, A. J. Leadbetter, and M. W. Stringfellow, *Phys. Rev. B* **27**, 1052 (1983).

¹³J. M. Carpenter and D. L. Price, *Phys. Rev. Lett.* **54**, 441 (1985).

¹⁴A. J. Leadbetter and A. C. Wright, *J. Non-Cryst. Solids* **7**, 23 (1972).

¹⁵U. Buchenau, *Z. Phys. B* **58**, 181 (1985).

¹⁶J. M. Carpenter and C. A. Pelizzari, *Phys. Rev. B* **12**, 2391 (1975).

¹⁷J. M. Carpenter, *J. Chem. Phys.* **46**, 465 (1967).

¹⁸S. C. Moss and D. L. Price, in *Physics of Disordered Materials*, edited by D. Adler, H. Fritzche, and S. R. Ovshinsky (Plenum, New York, 1985).

¹⁹R. Vacher and J. Pelous, *Phys. Rev. B* **14**, 823 (1976).

²⁰M. Rothenfusser, W. Dietsche, and H. Kinder, *Phys. Rev. B* **27**, 5196 (1983).

²¹A. C. Anderson, in *Amorphous Solids—Low Temperature Properties*, Ref. 1.

²²P. H. Gaskell and I. D. Tarrant, *Philos. Mag. B* **42**, 265 (1980).

²³M. D. Newton and G. V. Gibbs, *Phys. Chem. Minerals* **6**, 221 (1980).

²⁴P. H. Gaskell, *Trans. Faraday Soc.* **62**, 1505 (1966).

²⁵M. M. Elcombe, *Proc. Phys. Soc.* **91**, 947 (1967).

²⁶H. Grimm and B. Dorner, *J. Phys. Chem. Solids* **36**, 407 (1975).

²⁷M. E. Striefer and G. R. Barsch, *Phys. Rev. B* **12**, 4553 (1975).

²⁸R. Kulas and M. F. Thorpe, in *Structure and Excitation of Amorphous Solids (Williamsburg, Va., 1976)*, Proceedings of an International Conference on Structure and Excitation of

- Amorphous Solids, AIP Conf. Proc. No. 31, edited by G. Lugo-
vsky P. L. Galeener (AIP, New York, 1976).
- ²⁹N. Ahmad and W. A. Phillips (unpublished).
- ³⁰S. Alexander and R. Orbach, J. Phys. (Paris) Lett. **43**, L624
(1982).
- ³¹C. I. Nicholls and H. M. Rosenberg, J. Phys. C **17**, 1165
(1984).
- ³²J. C. Phillips, Phys. Rev. B **32**, 5356 (1985).
- ³³F. L. Galeener and A. C. Wright, Solid State Commun. **57**,
677 (1986).
- ³⁴U. Buchenau, Solid State Commun. **56**, 889 (1985).
- ³⁵L. Guttman and S. M. Rahman, Phys. Rev. B **33**, 1506 (1986).